scientific reports

Check for updates

OPEN

The signature based on interleukin family and receptors identified IL19 and IL20RA in promoting nephroblastoma progression through STAT3 pathway

Chen Ding[1,3], Hongjie Gao[2,3], Liting Zhang[1], Zhiyi Lu[1], Bowen Zhang[1], Ding Li[1] & Fengyin Sun[1]✉

Wilms tumor (WT) is a common renal malignancy in pediatric patients. Interleukin (receptors) (IL(R)s) play significant roles in tumor biology, however, their specific involvement in WT remains inadequately understood. We employed univariate Cox regression analysis to screen for certain IL(R) genes associated with prognosis and then analyzed their expression patterns. A prognostic model was constructed based on five selected IL(R)s using the LASSO Cox regression algorithm. To further elucidate the relationship between the prognostic model and the immune microenvironment, we conducted immune-related analyses. Additionally, we performed experiments to verify the roles of *IL20RA* and *IL19* in WT. Finally, CNV, methylation and pan-cancer analysis were performed for *IL19* and *IL20RA*. Our analysis ultimately identified five genes associated with prognosis: *IL20RA*, *IL19*, *IL24*, *IL11* and *IL17RD*. The prognostic model incorporating these five genes demonstrated robust predictive power in both training and validation cohorts. Notably, *IL19* and *IL20RA* were found to promote epithelial-mesenchymal transition (EMT) through the *STAT3/SNAIL* pathway, thereby contributing to tumor progression. Furthermore, significant differences in immune function and checkpoint expression were observed between the two groups. The high-risk group exhibiting a lower TIDE score, which suggests a potentially better response to immunotherapy. This study introduces a novel IL(R)-based prognostic signature for WT, highlighting *IL20RA* as a potential therapeutic target. These findings offer valuable insights for future studies on WT.

Keywords Bioinformatics, Wilms tumor, Interleukin (receptors), IL20RA, Immune infiltration, Epithelial-mesenchymal transition

Abbreviations

WT	Wilms tumor
IL(R)s	Interleukin (receptors)
TCGA	The Cancer Genome Atlas Program
DEGs	Differentially expressed genes
EMT	Epithelial-mesenchymal transition
LASSO	Least absolute shrinkage and selection operator
ROC	Receiver operating characteristic curve
AUC	The area under the ROC curve
TIDE	Tumor immune dysfunction and exclusion
COIP	Co-immunoprecipitation
CHIP	Chromatin immuno-precipitation
RMST	Restricted mean survival time

[1]Department of Pediatric Surgery, Qilu Hospital of Shandong University, 107 Wenhua West Road, Jinan 250012, China. [2]Department of Pediatrics, Qilu Hospital of Shandong University, Jinan, China. [3]Chen Ding and Hongjie Gao contributed equally to this work and share first authorship. ✉email: sunfengyin@qiluhospital.com

Nephroblastoma, also known as Wilms tumor (WT), is the most prevalent malignant kidney tumors in children worldwide. While the 5-year overall survival rates for patients with WT have reached 90%, the prognosis for certain WT subtypes remains poor[1]. Despite multimodality therapies, the most effective treatments are surgery, chemotherapy, and chemoradiation, which are accompanied by the risk of kidney dysfunction, recurrence, cardiotoxic side effects and so on[2]. Immunotherapy for WT is still in its early stages[3], so there is an urgent need to find novel therapeutic targets to reduce the occurrence of complications[4].

IL (R) families, as cytokines originally thought to be derived from white blood cells, are produced by multiple cell types and continuously interact with cells in the tumor microenvironment[5]. These cytokines are crucial in regulating inflammatory responses, maintaining stemness, promoting angiogenesis, exerting antiapoptotic effects, and increasing sensitivity to immunotherapy in tumor[6–10]. For instance, Treg-derived *IL10* acts on AML cells and enhances stemness through activation of the *IL10R/PI3K/AKT* pathway[11], and similarly, it functions via *JAK1/STAT1/NF-κB/Notch1* pathway in non-small cell lung cancer[12]. In melanoma, *IL10* acts as a negative regulator of T-cell activation and tumor immunity, thereby promoting immune escape of cancer cells[13]. *WT1* as the causative gene of Wilms tumor, was reported to promote the transcription of IL10[14]. Additionally, *IL11* binds to the *IL11* receptor and mediates therapy resistance and relapse through *JAK1/STAT4* pathway[15]. So far, combination immunotherapy including *IL-15* superagonist complex (ALT-803) and pegylated IL-10 has been assessed to improving the therapeutic outcome of *PD-1*[16,17].

Studies have explored IL (R)s expression and their role in tumors[18], but few studies focused on their role in nephroblastoma tumorigenesis. The present study constructed a IL(R)-based prognostic signature, effectively predicting nephroblastoma prognosis using univariate COX regression and lasso regression analysis. The risk score, derived from the expression of five signature genes, was closely related to immune status. Finally, we clinically verified the expression and functions of IL20RA and IL19 in Wit-49 cell line. Molecular biology experiments revealed that *IL19/IL20RA* are able to promoted EMT by activating the *STAT3/SNAIL* pathway. Consequently, our study introduces a novel prognostic indicator, with IL20RA emerging as a potential therapeutic target.

Results

The IL(R)s-based signature can predict the prognosis of patients with WT

Univariate Cox regression analysis based on the 96 IL(R)s was performed to identify genes associated with cancer prognosis, the forest plot showed the prognostic significance of five genes (*IL20RA, IL19, IL11*, *IL17RD and IL24*) in WT patients (Fig. 1A). In total, 4871 differentially expressed genes (DEGs) between tumor and normal samples were found in Wilms tumor (Fig. 1B), including 2848 upregulated DEGs (log FC > 2, $p < 0.05$) and 2023 downregulated DEGs (log FC < − 2, $p < 0.05$). Figure 1C illustrated the expression of five genes in normal and WT samples.

We next divided the data randomly into a training and validation set in a ratio of 8:2. LASSO Cox regression algorithm was applied to develop a signature in the training set (Fig. 1D, E). A riskScore was calculated for each patient in the training and testing sets. We then grouped patients into groups of high and low risk according to the median riskScore. The K-M curves ($p < 0.05$, Fig. 1F, I) and ROC curves (Fig. 1G, H) suggested that the riskScore showed good power in predicting OS in the training and validating dataset. Figure 2A, B suggested that patients in the high-risk group had a higher death rate and higher expression of *IL11, IL24, IL19* and *IL20RA* than those in the low-risk group.

Construct a prognosis model based on five IL(R)s

Univariate and multivariate Cox regression of riskScore and clinicopathological characteristics showed the riskScore, age and clinical stage were independent prognostic predictors (Fig. 3A, B). The nomogram was developed based on the multivariate Cox regression analysis of clinical variables to predict the combined effect of predictors at 1, 3, and 5 years (Fig. 3C). Moreover, calibration curves indicated the sensitive detection and accuracy of the nomogram for 1, 3 and 5-year overall survival (Fig. 3D). AUC analyses demonstrated that the discrimination performance of riskScore was significantly better than that of the other prognostic factors (Fig. 3E). To validate the prognostic power of riskScore, we calculated the 10-year RMST of the two risk groups, and the mean OS RMST difference was 760.075 days (range 241.473 to 1278.68 days, $p = 0.004$, Table S1 and Figure S1).

There are significant correlations between IL(R)s signature and clinical characteristics and prognosis

The riskScore was strongly associated with clinical stage ($p < 0.05$, Fig. 4B). *IL17RD* expression decreases with the increase in clinical stages ($p < 0.05$, Fig. 4A). Moreover, we found significantly high *IL11, IL24, IL19* and *IL20RA* expression and high risk score in cases of tumor progression (Fig. 4C, D). There was a close protein–protein interaction among the five signature genes, with a confidence score of 0.700 (Fig. 4E). Among these genes, IL19 and IL24 served as ligands for IL20RA[19]. Kaplan–Meier curves showed a distinct association between the five genes and overall survival (Fig. 4F–J), among them, *IL20RA* had the highest hazard ratio (HR = 2.9, $p < 0.001$, Fig. 4H). The results of the subgroup analysis showed the prognostic significance of IL19 expression levels was not significant in patients either under or older than 5 years. Similarly, for IL11 and IL7RD, the prognostic role of their expression levels was also not significant in patients older than 5 years. The p-values for interaction were greater than 0.05, indicating no statistically significant association between age and the prognostic effect of these gene expression levels (Table S2).

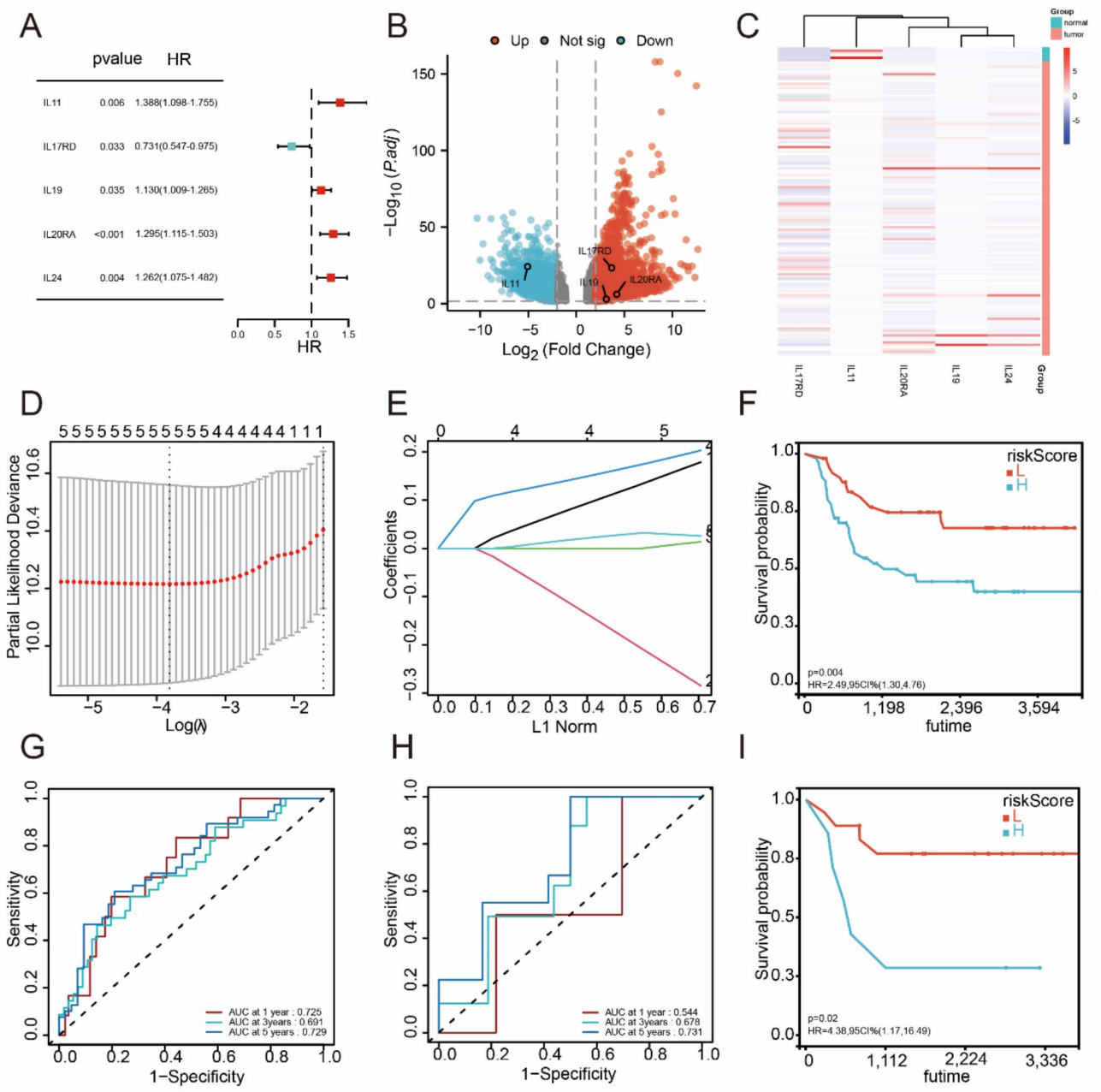

Fig. 1. Construction of genes signature based on IL(R)s. (**A**) Univariate Cox regression analysis was performed, and 5 IL(R)s were statistically significant. (**B**) Volcano plot of DEGs in WT ($p < 0.05$ and $|\log FC| \geq 2$). (**C**) Heatmap of 5 genes between normal kidney and WT tissues. (**D**) Penalty plot of the LASSO model, which reflected optimum value according to the minimum and 1-SE criterion. (**E**) LASSO plot showed the trajectory of each independent variable. Survival analysis and ROC analysis of riskScore in training sets (**F**, **G**) and validation set (**H**, **I**). DEGs, differentially expressed genes; WT, Wilms tumor; logFC, log2 fold change; ROC, receiver operating characteristic.

Explore immune landscapes of patients in two groups

In terms of the immune function, patients with a high riskScore had a higher interleukins score compared to the low-risk group. Conversely, TCR signaling pathway and *TGFb* family member pathway were enriched in the low-risk group (Fig. 5A). We next compared the immune scores of the two subtype samples using the MCPcounter tool. T cells and Neutrophils showed higher abundance in low-risk group (Fig. 5B). Noticeably, immune checkpoint molecules, including *CD160, TNFSF4, and IFNA2*, showed higher expression in the high-risk group. And *TLR4, ENTPD1 and CD44* were significantly up-regulated in the low-risk group (Fig. 5D). We also infer the immunotherapeutic response of WT patients by using the TIDE web program. Patients with a low riskScore were predicted to had a higher TIDE score ($p < 0.05$, (Fig. 5C), and patients who responded to immunotherapy had higher riskScores (Fig. 5E).

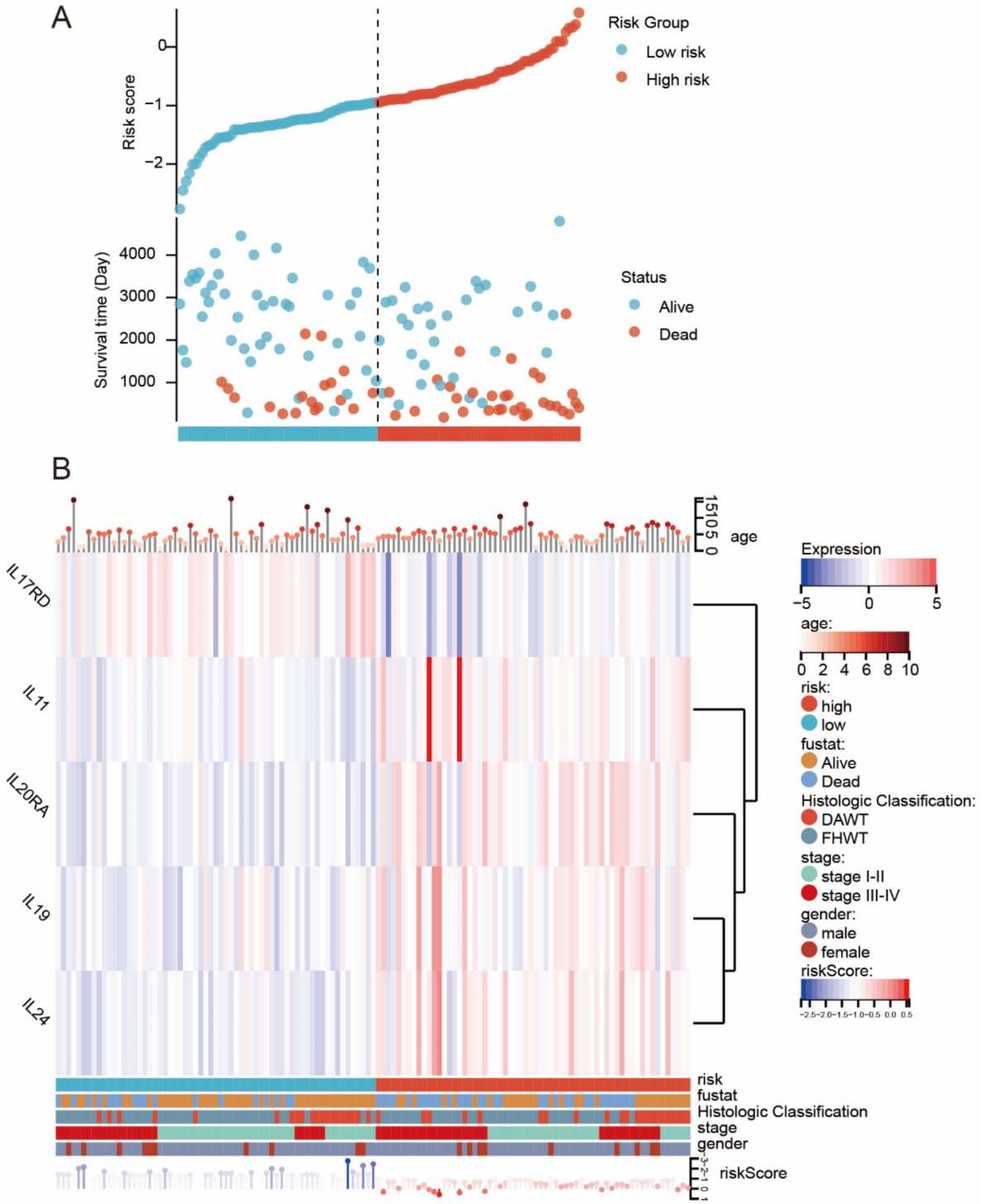

Fig. 2. Distribution of the riskScore. (**A**) The association of riskScore and survival status. (**B**) Gene expression heatmap. DAWT, diffusely anaplastic Wilms tumor; FHWT, favorable histology Wilms tumor.

WT patients are clustered according to the differential gene expression between two groups

To further interrogate the characteristics of the five-gene signature, we screened for 133 differentially expressed genes between high-risk and low-risk groups ($|\log2FC| > 1$, adjusted $p < 0.05$). Among them, 32 genes significantly associated with patient prognosis were identified through univariate Cox regression analysis ($p < 0.05$, Table S3). We performed an unsupervised clustering based on the 32 genes (Fig. 6A, B). Patients in cluster 1 had a significantly worse overall survival (Fig. 6C) and lower ESTIMATE score (Fig. 6G). Immunosuppressive genes

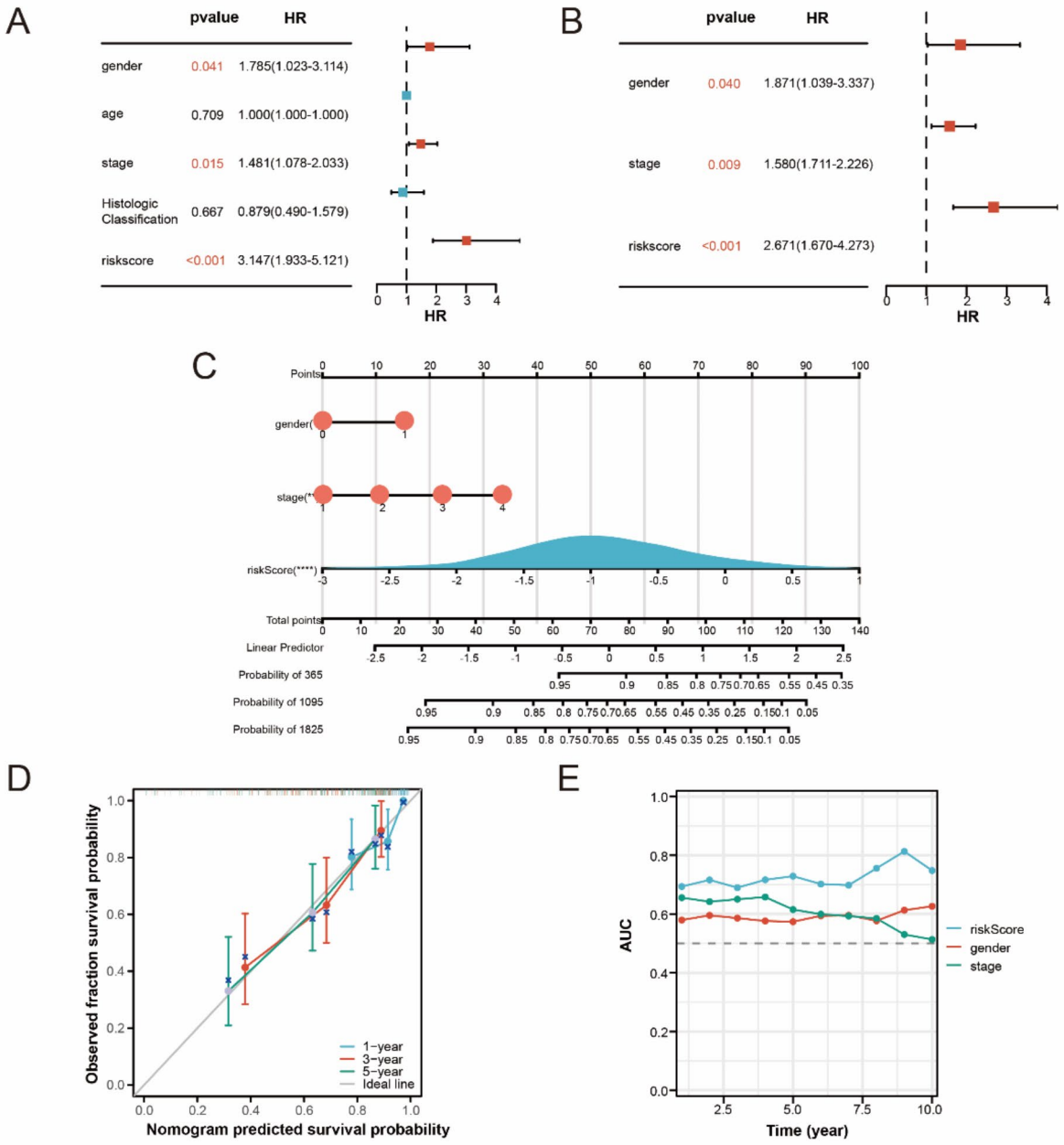

Fig. 3. Construction and evaluation of the nomogram. The univariate (**A**) and multivariate (**B**) Cox regression analysis of risk factors in Wilms tumour. (**C**) Nomogram containing the five-gene signature and clinical characteristics to evaluate prognosis in WT (1-, 3-, and 5-year survival rates). (**D**) The calibration plot showed that the nomogram was well calibrated. (**E**) AUC curves of the five-gene signature and clinical characteristics for 1–10 years. AUC, Area Under Curve.

such as immune checkpoints *BTNL2, LAG3 and PDCD1* were highly expressed in Cluster 1, while *CD200R1, CD40LG, CD44, CD48 and CD86* were significantly overexpressed in Cluster 2 (Fig. 6D). A variety of immune functions, including chemokines, cytokines and TGFb family member were significantly enriched in Cluster 2 (Fig. 6E). Moreover, T cells, DCs and Fibroblasts showed higher abundance in Cluster 2 (Fig. 6F).

IL20RA is highly expressed in nephroblastoma and correlates with poor prognosis

Among the five signature genes, *IL19* and *IL20RA* function as a ligand–receptor pair, exhibit strong prognostic and staging correlations, and are associated with hypoxic conditions in breast cancer and vascular disease[20,21]. Initially, we confirmed the overexpression of *IL19* and *IL20RA* in Wit-49 cell lines by real-time quantitative PCR (Fig. 7A, C). It was found the level of the two genes increased with the prolonged period of hypoxia (Fig. 7B, D).

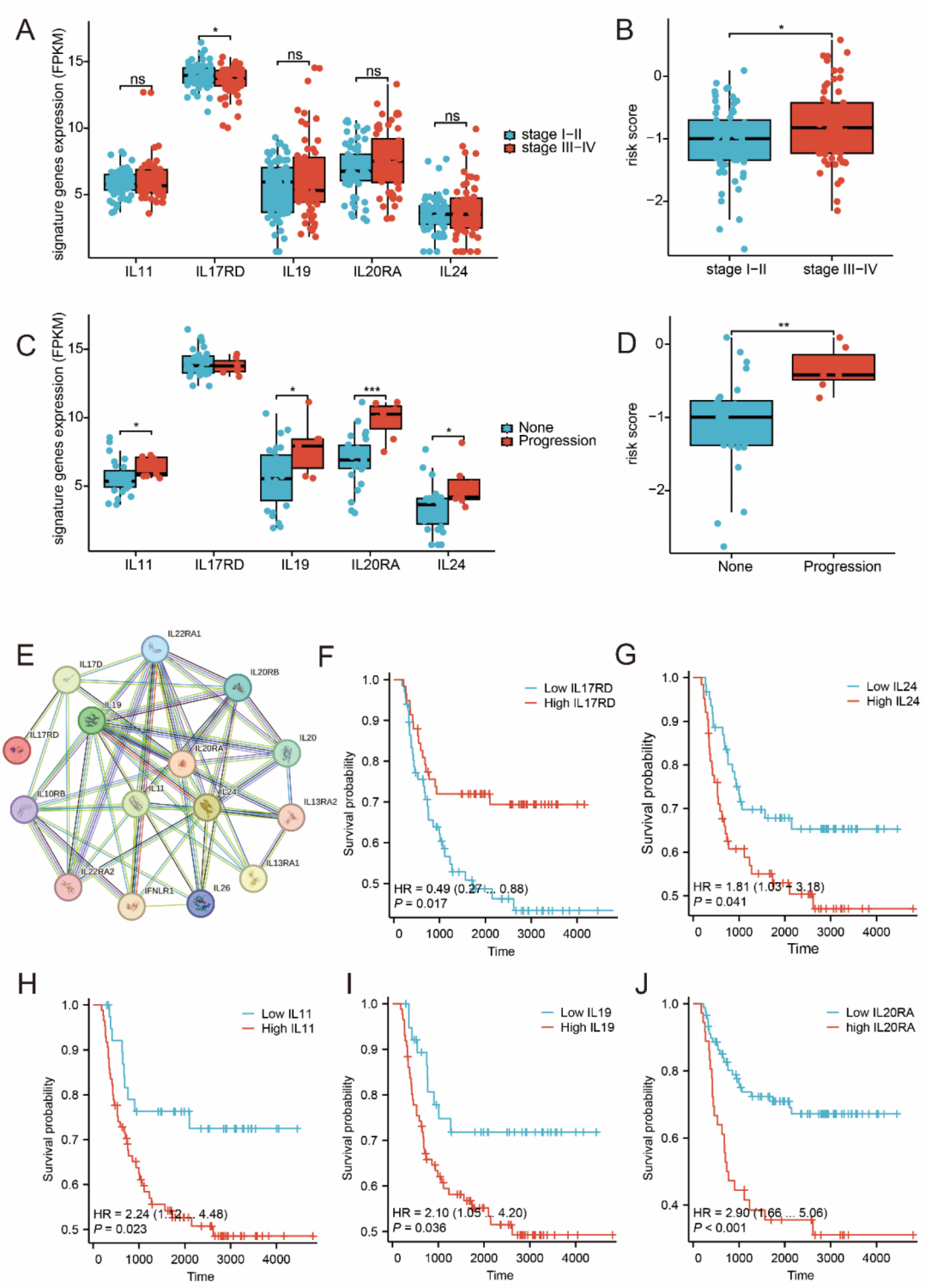

Fig. 4. Clinical correlation analysis of five signature genes. (**A**, **B**) The distribution of riskScore and genes expression in different clinical stage was plotted in Box plots. (**C**, **D**) Correlation between five signature genes expression and riskScore and clinical progression. (**E**) PPI (Protein–Protein Interactions) of the signature genes (STRING database). (**F**–**J**) The Kaplan–Meier curves of OS of five genes in entire cohort. *$p<0.05$; **$p<0.01$; ***$p<0.001$; ns, not significant.

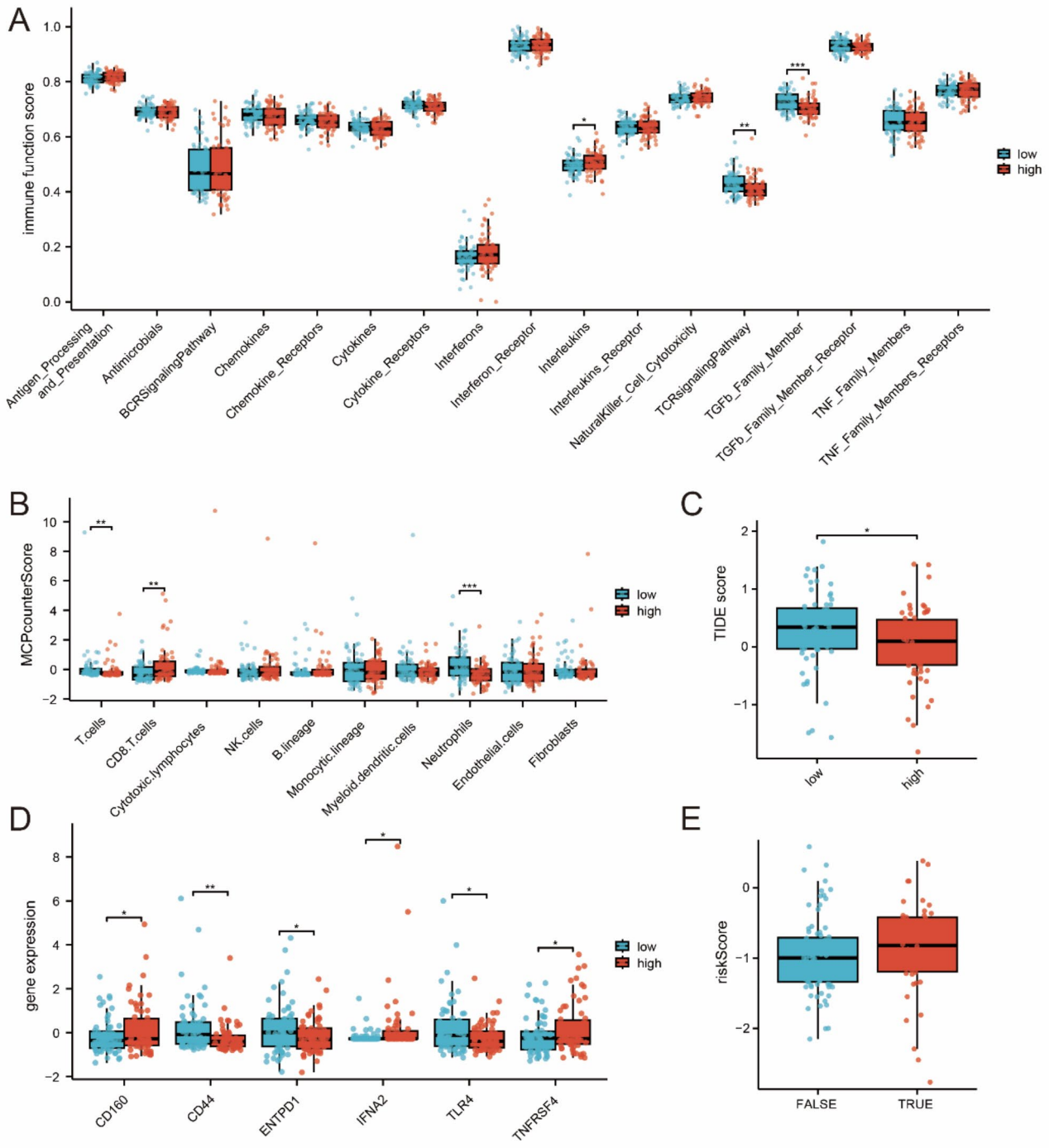

Fig. 5. Associations between the immune signature and immune infiltration. (**A**) Distribution of immune function in high- and low-risk subgroups. (**B**) Box plot showing the differences of immune cell infiltration. (**C**) The differences of TIDE score between high-risk group and low-risk groups. (**D**) Distribution of immune checkpoint molecules' expression between the high- and low-risk subgroups. (**E**) Distribution of riskScore between different immunotherapy responses. $^{*}p < 0.05$; $^{**}p < 0.01$; $^{***}p < 0.001$.

Furthermore, immunohistochemical analysis showed an abnormally elevated expression of IL20RA in tumor tissues ($p < 0.01$, Fig. 7E, F).

Knockdown of *IL19* dramatically suppressed Wit-49 cell proliferation, as demonstrated by CCK8 assay (Fig. 8A, B). Transwell assays (Fig. 8C, D) and wound-healing assays (Fig. 8E, F) were used to test the inhibitory effect of *IL19* knockdown on cell migration. *IL20RA* has the same function as *IL19* on cell proliferation and migration (Fig. 9).

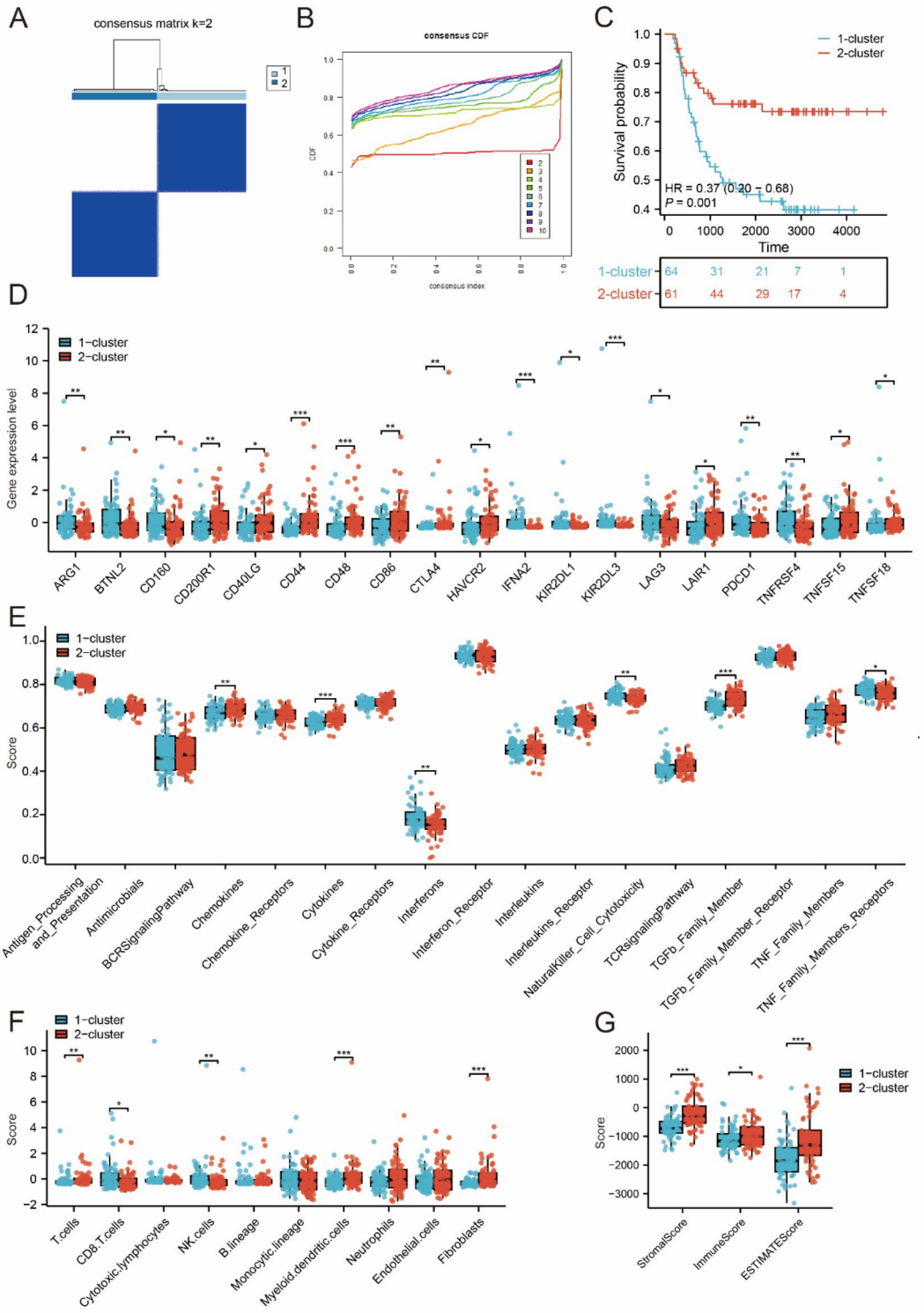

Fig.6. Identification and analysis of IL(R)s-Associated Clusters. (**A**, **B**) The optimal consensus clustering matrix with k = 2. (**C**) There was a difference between the KM survival curves of the two clusters. Distribution of immune checkpoint molecules' expression (**D**), immune function (**E**), immune cell infiltration (**F**) and ESTIMARE score (**G**) in two clusters. $^{*}p < 0.05$; $^{**}p < 0.01$; $^{***}p < 0.001$.

IL19/IL20RA promote cell proliferation and migration by STAT3 signal transduction

Previous studies have uncovered that the *IL10* gene family plays a crucial role in regulating cell growth and survival via *JAK/STAT* pathway[22,23]. In recent years, particular attention has been given to IL19 and IL20RA(B) in the context of various systemic diseases. Within the cardiovascular system, IL19 is implicated in promoting

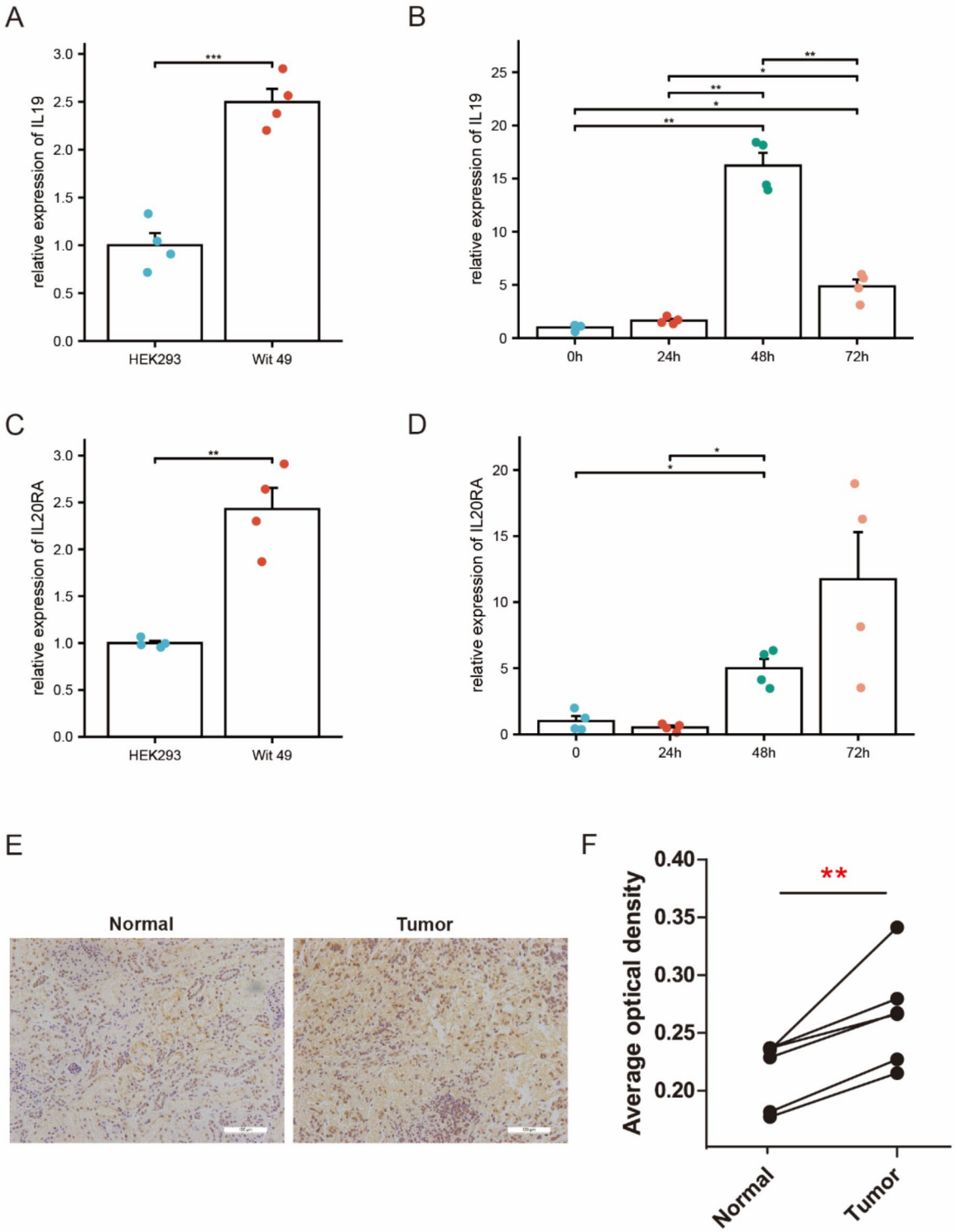

Fig. 7. Validation of IL19 and IL20RA expression. (**A**, **B**) IL19 presented high expression in Wit 49 cells and were significantly increased after culturing in hypoxia. (**C**, **D**) IL20RA presented high expression in Wit 49 cells and were significantly increased after culturing in hypoxia. (**E**) Representative diagram of immunohistochemistry of IL20RA in normal and tumor tissues. (**F**) Pairing analysis of the mean optical density between the two sample groups. $^{*}p < 0.05$; $^{**}p < 0.01$; $^{***}p < 0.001$.

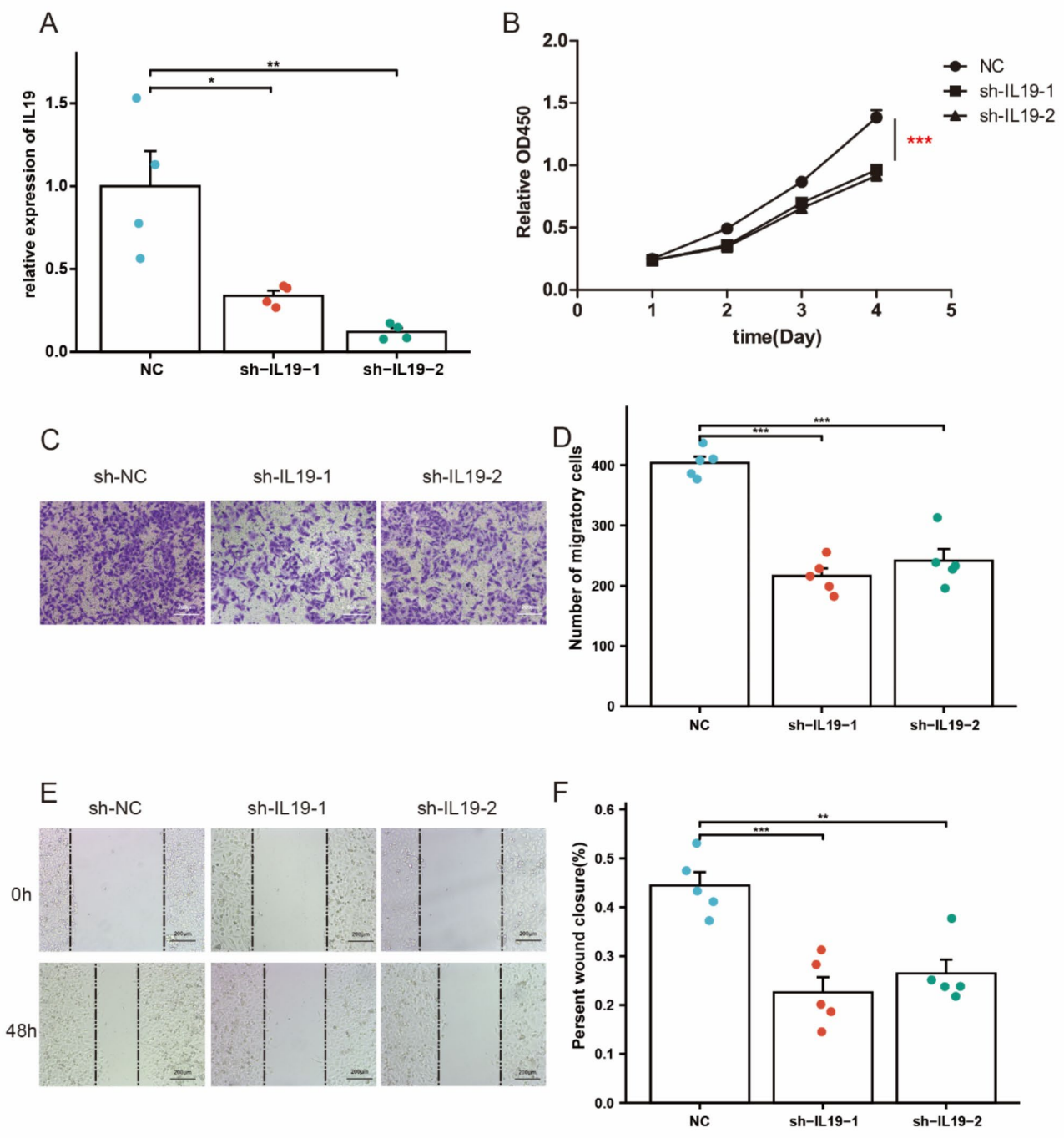

Fig. 8. IL19 Effects on tumor cell Function. (**A**) Knockdown efficiency measured by RT-qPCR. (**B**) The absorbance was measured at 24, 48, 72, and 96 h. (**C**, **D**) Number of cells passing through the membrane after 24 h. (**E**, **F**) Wound healing capacity of cells within 48 h. $^{*}p < 0.05$; $^{**}p < 0.01$; $^{***}p < 0.001$.

macrophage polarization by regulating cholesterol efflux, thereby accelerating the progression of atherosclerotic plaques[24]. Furthermore, IL19 interacts with immune mechanisms to facilitate neovascularization through the activation of STAT3[25]. This interaction with the STAT3 pathway is also evident in chronic respiratory diseases, where IL19 plays a significant role[26]. In addition to this, IL19/IL20RB complex is involved in mediating bone metastasis in lung cancer through JAK1/STAT3 signaling[27]. These findings underscore the multifaceted roles of IL19, IL20RA(B) and STAT3 pathway in various pathological processes, highlighting their potential as therapeutic targets. Hence, we next evaluated the interaction among *IL19, IL20RA* and *STAT3* activation. Knockdown of *IL19* significantly decreased *IL20RA* expression and reduced *STAT3* phosphorylation (Fig. 10A–

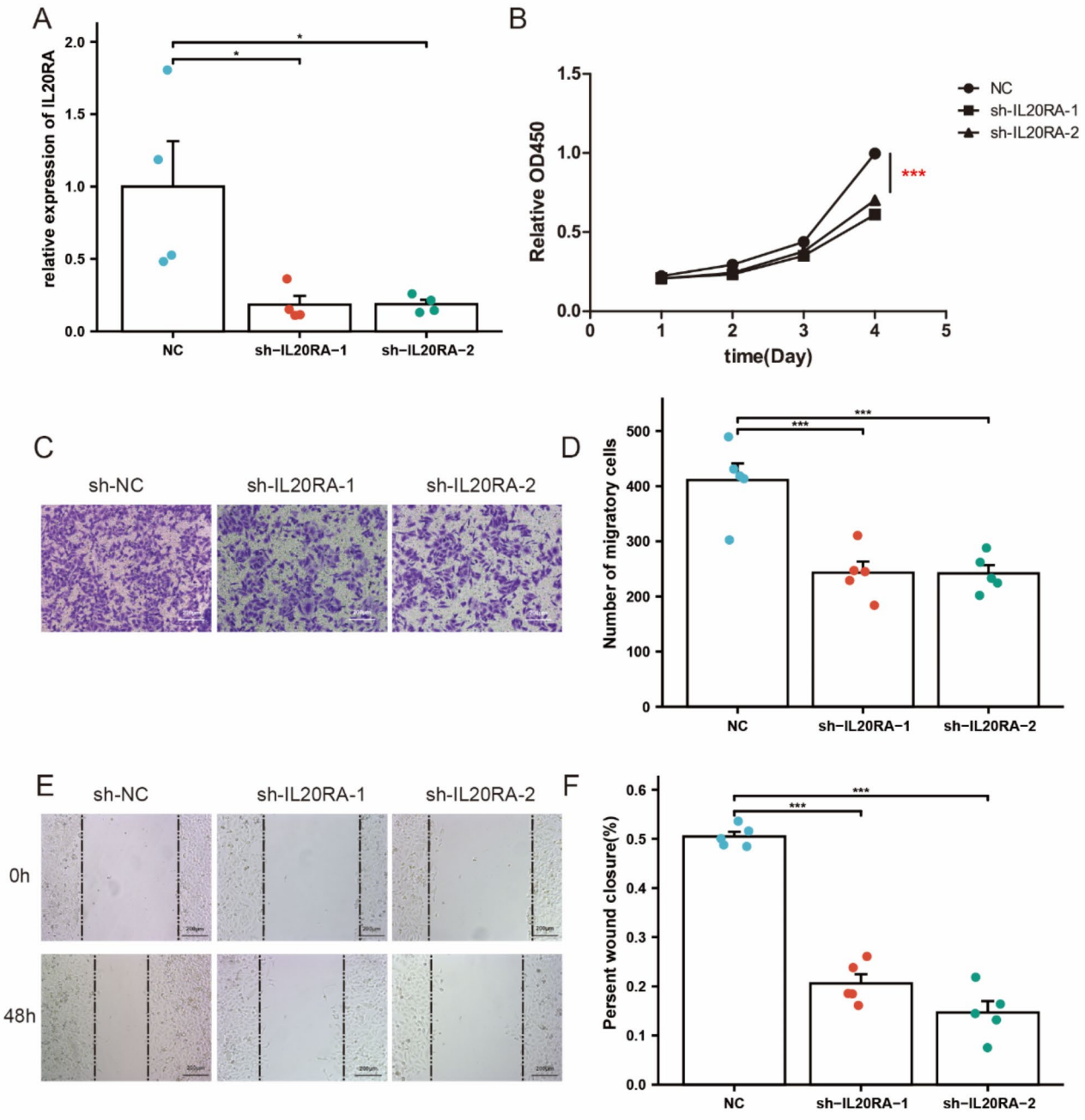

Fig. 9. IL20RA Effects on tumor cell Function. (**A**) Knockdown efficiency measured by RT-qPCR. (**B**) The absorbance was measured at 24, 48, 72, and 96 h (**C**, **D**) Number of cells passing through the membrane after 24 h. (**E**, **F**) Wound healing capacity of cells within 48 h. $^{*}p < 0.05$; $^{***}p < 0.001$.

C). *IL19* overexpression significantly promoted cell proliferation and migration, and *IL20RA* knockdown attenuates the function of *IL19* (Fig. 10D–H).

Additionally, STAT3 phosphorylation levels increased with IL20RA overexpression (Figure S2) and decreased when IL20RA was knocked down (Fig. 11A–C). Functional experiments suggests that *STAT3* phosphorylation inhibitor (Stattic) was able to rescued tumorigenicity of *IL20RA* (Fig. 11D–H). Taken together, our results suggest that IL20RA is upregulated by IL19 and promotes tumor progression by activating *STAT3*.

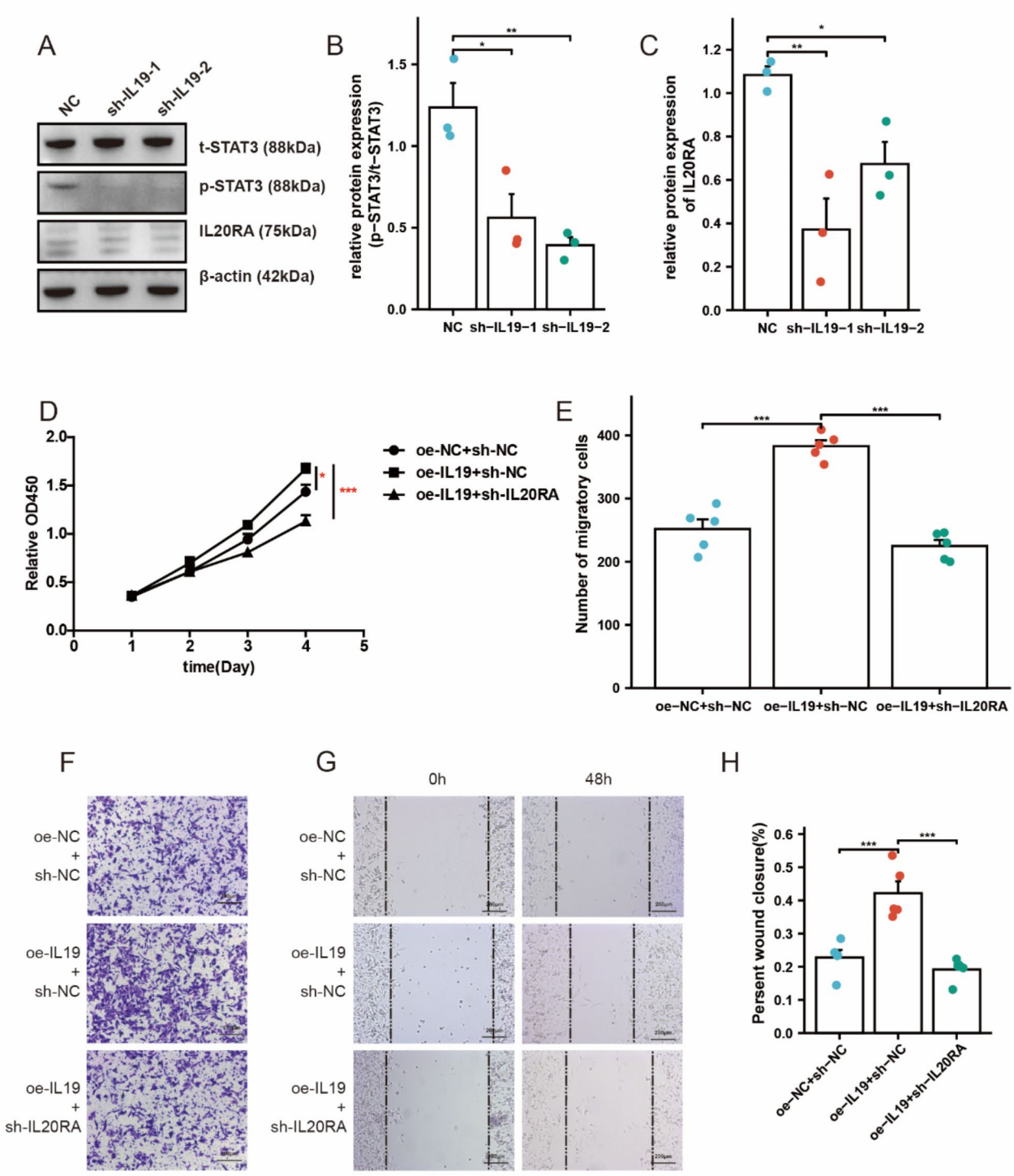

Fig. 10. Rescue assay with oe-IL19 and sh-IL20RA. (**A**–**C**) Western blots demonstrated a decrease of IL20RA and p-STAT3 in IL19-knockdown Wit 49 cells. (**D**) Cell proliferation was assessed via CCK-8 assay. (E–H) Transwell assay and scratch assay were used to evaluate cell migration function. $^{*}p < 0.05$; $^{**}p < 0.01$; $^{***}p < 0.001$.

IL20RA directly binds to STAT3 and activates Snail transcription

To investigate how *IL20RA* functions through phosphorylation of *STAT3*, we predicted the binding partners of *IL20RA* using the databases Hitpredict (Table S4) and BioGRID (Table S5). Our analysis suggested a direct interaction between IL20RA and STAT3. To validate this interaction, we transfected 293 T cells with a Flag-IL20RA expression plasmid and conducted co-immunoprecipitation (COIP) assays, which confirmed the direct

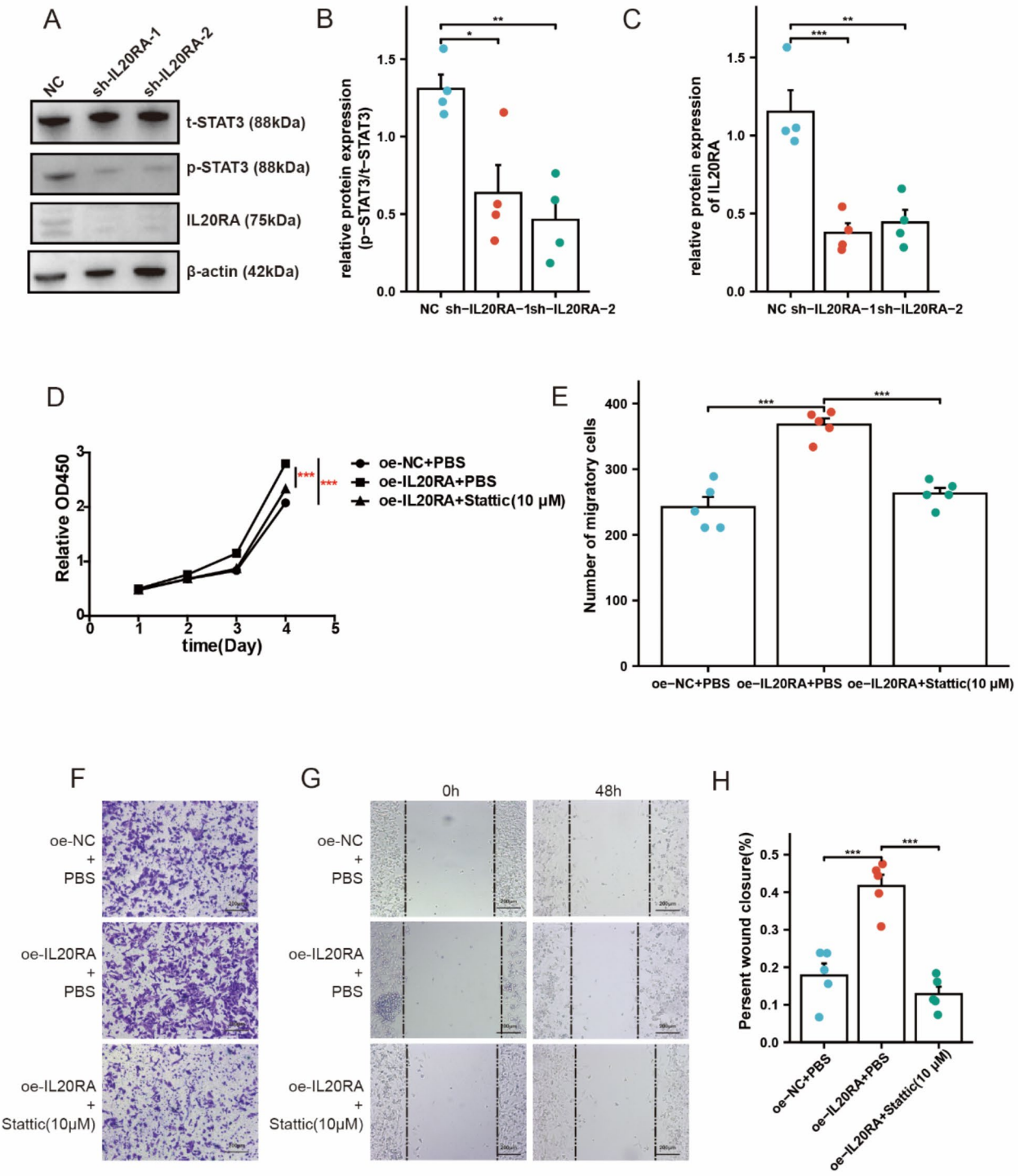

Fig. 11. Rescue assay with oe-IL20RA and STAT3 specific inhibitor. (**A**–**C**) Western blots demonstrated a decrease of IL20RA and p-STAT3 in IL20RA-knockdown Wit 49 cells. (**D**) Cell proliferation was assessed via CCK-8 assay. (**E**, **H**) Transwell assay and scratch assay were used to evaluate cell migration function. $^{*}p<0.05$; $^{**}p<0.01$; $^{***}p<0.001$.

binding of *IL20RA to STAT3* (Fig. 12A). Given previous reports on IL20RA's involvement in EMT[28] and its role in promoting tumor metastasis[27], we further investigated whether IL20RA promoted EMT via STAT3 in Wilms tumor. We identified STAT3 binding sites within the promoter region of *Snail* using JASPAR databases (Fig. 12B). CHIP-qPCR experiment revealed two binding sites, with reduced binding observed upon IL20RA knockdown

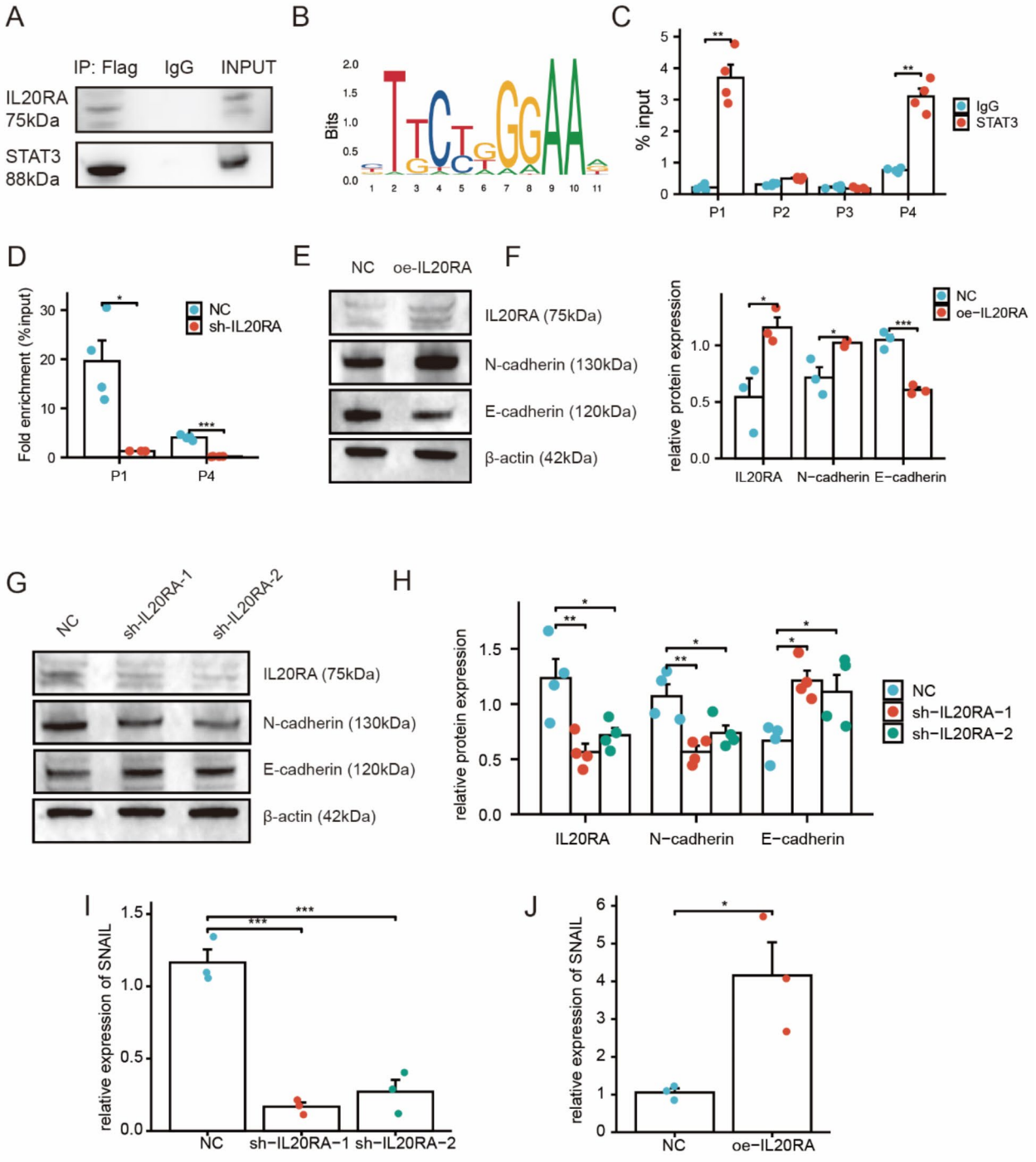

Fig. 12. Exploration of downstream mechanisms of IL20RA. (**A**) IL20RA was coimmunoprecipitated (coIP) with STAT3. (**B**) The sequence in gene promoter that is recognized by STAT3 (Jasper). (**C**) ChIP-qPCR showed that STAT3 had binding sites in the promoter region of SNAIL gene. (**D**) Compared with the control group, the binding signal of STAT3 to the SNAIL promoter region was significantly reduced after knockdown of IL20RA. (**E**, **F**) A decrease of E-cadherin and increase of N-cadherin after IL20RA was overexpressed. (**G**, **H**) Western blots demonstrated a decrease of N-cadherin and increase of E-cadherin after IL20RA was knocked down. (**I**, **J**) RT-qPCR results showed that Snail expression was significantly reduced upon silencing of IL20RA and increased by overexpressed of IL20RA. $^{*}p < 0.05$; $^{**}p < 0.01$; $^{***}p < 0.001$.

(Fig. 12C, D). Additionally, IL20RA was found to enhance the expression of *N-cadherin* and suppressed the expression of *E-cadherin* (Fig. 12E–H). RT-qPCR analysis indicated that overexpression of *IL20RA* upregulated Snail expression whereas knockdown of *IL20RA* led to a reduction in *Snail* expression (Fig. 12I, J). Finally, we confirmed the pro-tumorigenic effects of IL20RA in vivo (Fig. 13).

Genomics and pan-cancer analysis of IL19 and IL20RA

To investigate potential mechanisms underlying the transcriptional enrichment of IL19 and IL20RA in WT, we analyzed copy number variation and DNA methylation at these loci using cBioportal for Cancer Genomics database (https://www.cbioportal.org/). Among the 125 WT-patients with CNV data, 5 had an IL19 amplification and suffered from Progression and relapse (Fig. 14A). There was a negative correlation between the degree of DNA methylation and the gene expression (Fig. 14B, C). Overexpression of IL19 and IL20RA were differentially expressed and associated with prognosis in various human cancer types, as prompted by Sangerbox tool (http://vip.sangerbox.com/login.html, Fig. 14D, E, Figure S3).

Discussion

Nephroblastoma or Wilms tumor is one of the most common pediatric cancers[29], necessitating a multimodal treatment approach involving surgery, chemotherapy, and radiotherapy as per the SIOP and COG regimens[30]. Despite the efficacy of current treatment modalities, patients often experience long-term complications post-25 years from diagnosis[31], underscoring the critical need for early diagnostics and more effective therapeutic strategies.

Over the past few years, numerous studies have demonstrated the role of Interleukin in tumor development and progression. However, most studies have focused on the mechanisms of IL(R)s[32–34], and limited studies have investigated their prognostic significance in Wilms tumor[35]. Therefore, in this study, we identified 35 differentially expressed IL(R)s in the TARGET-WT database and utilized univariate COX and LASSO regression to construct a prognostic model based on five genes: *IL11, IL19, IL24 IL20RA, IL17RD*. Subsequently, univariate and multivariate COX regression analyses were carried out in conjunction with clinical data. Nomogram, ROC

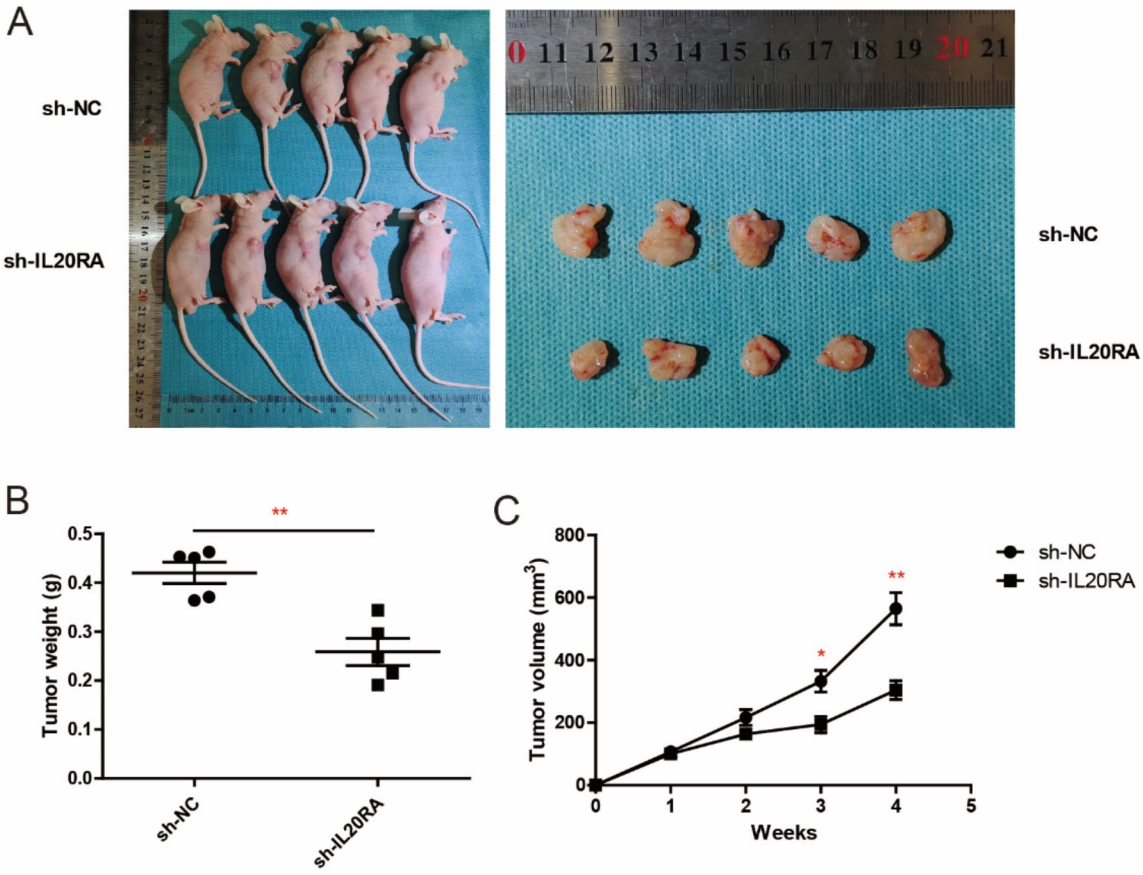

Fig. 13. Tumorigenesis of nude mice in two groups. (**A**) Tumorigenesis in nude mice in the sh-NC group (top) and sh-IL20RA group (bottom). (**B**) Comparison of tumor tissue weight between the two groups. (**C**) Growth chart of the tumors. *$p < 0.05$; **$p < 0.01$.

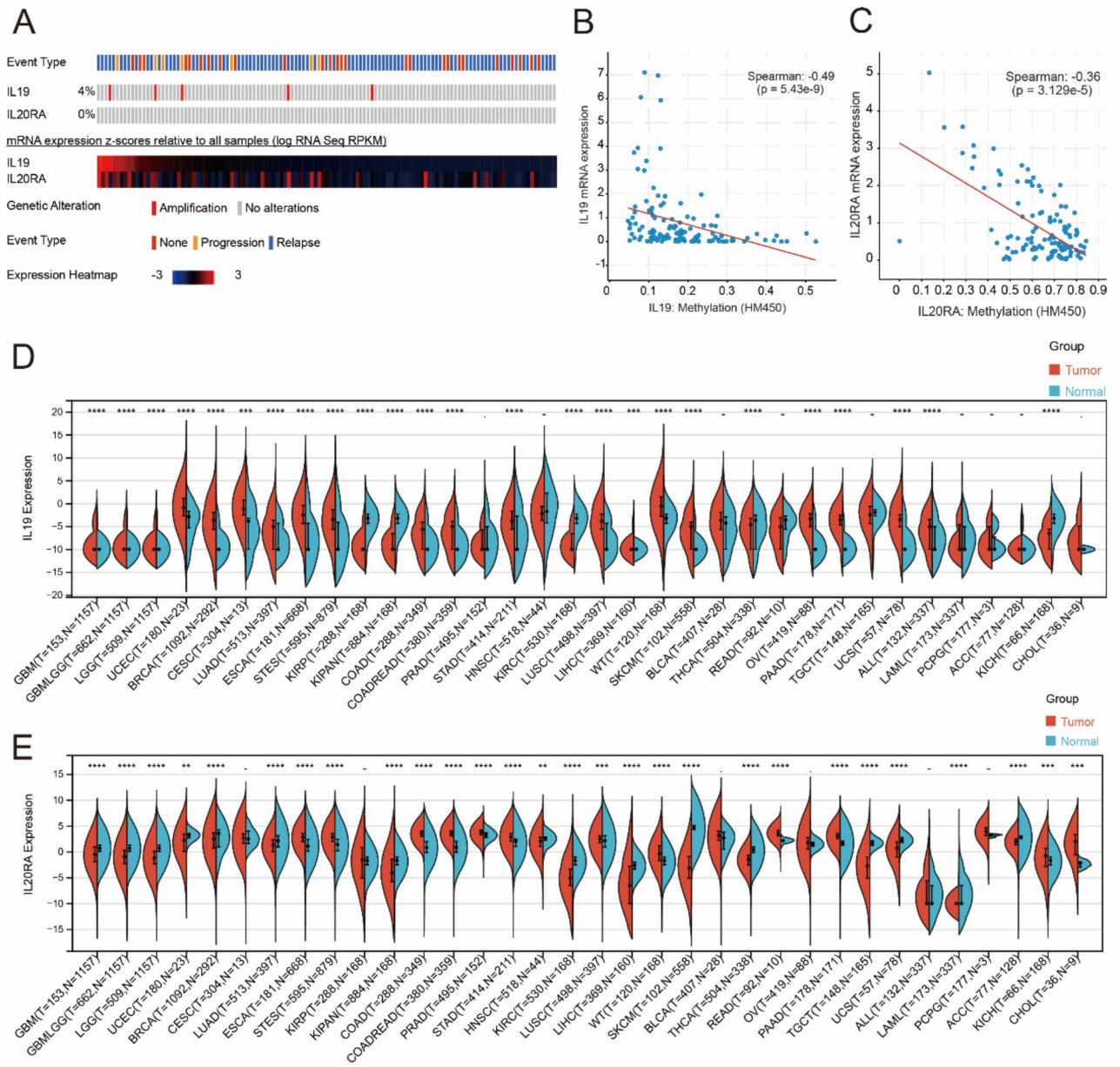

Fig. 14. Genetic alterations of IL19 and IL20ra in WT and gene expression profiles across pan-cancers. (**A**) Copy number variation results for IL19 and IL20RA. (**B**, **C**) Scatter plot showing the correlation between gene expression and methylation levels. The difference of IL19 (**D**) and IL20RA (**E**) in Pan-cancer. TCGA-ACC, Adrenocortical carcinoma; TCGA-BLCA, Bladder Urothelial Carcinoma; TCGA-BRCA, Breast invasive carcinoma; TCGA-CESC, Cervical squamous cell carcinoma and endocervical adenocarcinoma; TCGA-CHOL, Cholangiocarcinoma; TCGA-COAD, Colon adenocarcinoma; TCGA-COADREAD, Colon adenocarcinoma/Rectum adenocarcinoma Esophageal carcinoma; TCGA-DLBC, Lymphoid Neoplasm Diffuse Large B-cell Lymphoma; TCGA-ESCA, Esophageal carcinoma; TCGA-FPPP, FFPE Pilot Phase II; TCGA-GBM, Glioblastoma multiforme; TCGA-GBMLGG, Glioma; TCGA-HNSC, Head and Neck squamous cell carcinoma; TCGA-KICH, Kidney Chromophobe; TCGA-KIPAN, Pan-kidney cohort (KICH + KIRC + KIRP); TCGA-KIRC, Kidney renal clear cell carcinoma; TCGA-KIRP, Kidney renal papillary cell carcinoma; TCGA-LAML, Acute Myeloid Leukemia; TCGA-LGG, Brain Lower Grade Glioma; TCGA-LIHC, Liver hepatocellular carcinoma; TCGA-LUAD, Lung adenocarcinoma; TCGA-LUSC, Lung squamous cell carcinoma; TCGA-MESO, Mesothelioma; TCGA-OV, Ovarian serous cystadenocarcinoma; TCGA-PAAD, Pancreatic adenocarcinoma; TCGA-PCPG, Pheochromocytoma and Paraganglioma; TCGA-PRAD, Prostate adenocarcinoma; TCGA-READ, Rectum adenocarcinoma; TCGA-SARC, Sarcoma; TCGA-STAD, Stomach adenocarcinoma; TCGA-SKCM, Skin Cutaneous Melanoma; TCGA-STES, Stomach and Esophageal carcinoma; TCGA-TGCT, Testicular Germ Cell Tumors; TCGA-THCA, Thyroid carcinoma; TCGA-THYM, Thymoma; TCGA-UCEC, Uterine Corpus Endometrial Carcinoma; TCGA-UCS, Uterine Carcinosarcoma; TCGA-UVM, Uveal Melanoma; TARGET-OS, Osteosarcoma; TARGET-ALL, Acute Lymphoblastic Leukemia; TARGET-NB, Neuroblastoma; TARGET-WT, High-Risk Wilms Tumor. $^{**}p < 0.01$; $^{***}p < 0.001$; $^{****}p < 0.0001$.

curves and calibration curves were drawn, revealed the prognostic value of the model. Notably, patients in the low-risk group exhibited better overall survival, with higher TCR signaling pathway enrichment scores, which may potentially link to elevated *IL17RD* levels. Further analyses indicated the detrimental role of *IL20RA* in disease progression.

Moreover, investigations into the tumor microenvironment of Wilms tumor have gained traction in recent years. Xiao-Mao Tian et al.[36] constructed an immune-related prognostic model and shed light on the function of the key gene *NRP2*. Similarly, the model developed by Higgs et al. demonstrated a close relationship between DNA repair-related genes and anti-tumor immunity[37]. Our study delved into the correlation between the five-gene signature and the TME, revealing significant enrichment of the TCR signaling pathway and TGFb family member pathway in the low-risk group. Additionally, immune checkpoints such as *CD160, TNFSF4,* and *IFNA2* were highly expressed in the high-risk group ($p < 0.05$), indicating the potential correlation between our five-gene signature and TME. Next, we predicted the response to immunotherapy of patients in both groups using the TIDE score, finding that the high-risk group had a lower score ($p < 0.05$), which may indicate a better response to immunotherapy. These findings underscore the clinical relevance of our five-gene signature in guiding treatment for Wilms tumor patients.

We separately analyzed each of our five gene signatures, and *IL19* and *IL20RA* were selected for experimental validation due to their interaction and strong correlation with prognosis. Experimental validations including the CCK-8 assay, colony formation assay and transwell assay, highlighted their roles in tumor proliferation, migration and invasion through *STAT3* pathway. The literature indicates that hypoxia triggers an upregulation of IL19 expression in breast cancer cells[20], which subsequently activates pathways such as IL-1β, IL-6, MMP2, and MMP9 within tumor cells[20]. IL20RA exhibits a complex role in tumors. It has been reported as a tumor suppressor and inhibit metastasis in ovarian[38], colon[39], bladder[40] and lung-like cancers[41]. Conversely, studies in colorectal[28] and breast cancer[42] have identified IL20RA as a carcinogenic factor promoting tumor progression. In breast cancer, IL20RA enhances cell stemness through the JAK1-STAT3-SOX2 signaling pathway and regulates PD-L1 expression, affecting the immune microenvironment. Wenjuan Gao et al. combined IL20RA-targeted nanoparticles with anti-PD-L1 antibody to improve the chemotherapeutic efficacy in a breast cancer[42]. Additionally, *IL20RA* is regulated by super enhancers and is linked to the proliferative migration and epithelial-mesenchymal transition (EMT) pathways, specifically involving *Snail* and *Slug*, in colorectal cancer[28]. Our pan-cancer analysis (Fig. 14E) revealed that IL20RA expression varies significantly across cancer types, which may explain its dual functions. IL20RA was downregulated in bladder and ovarian cancers ($p > 0.05$), and this trend aligns with previous reports of its tumor-suppressive effects, though further validation is required. In colorectal adenocarcinoma, IL20RA expression was significantly upregulated, which may be associated with super-enhancer-mediated transcriptional activation and subsequent promotion of EMT, as previously reported.

Overall, most studies have shown that IL19, IL20RA are inextricably linked to the STAT pathway, particularly STAT3. Beyond neoplastic diseases, IL20RA is implicated in the IL20RA-mediated IFN/STAT2 pathway in colitis[43], and contributes to increased intraocular pressure through STAT1 and 3 phosphorylation[44]. Our findings confirmed the direct interaction of *IL20RA* with *STAT3* and its involvement in EMT regulation. Knockdown of IL20RA resulted in decreased levels of SNAIL and N-cadherin, alongside increased E-cadherin levels, aligning with existing literature.

In summary, this study established a prognostic model based on IL(R)s and elucidated its association with the immune microenvironment. Additionally, our findings underscored the role of IL19/IL20RA in promoting EMT through STAT3 activation. However, there are still some limitations: (I) firstly, all the data used to construct the model are from the database, and there is a lack of external validation due to insufficient data availability; (II) In addition, while the mechanism of IL19/IL20RA was explored through in vitro studies, there was a lack of further validation in vivo experiments. (III) Finally, the functions of *IL11, IL24* and *IL17RD* need to be further explored. Future research should address these identified limitations to enhance the clinical applicability of our findings.

Conclusion

This study presents a novel prognostic signature for WT based on five IL(R)s. Our model exhibits robust predictive power, particularly highlighting the roles of *IL19* and *IL20RA* in driving EMT through the *STAT3/SNAIL* signaling pathway. These findings not only identify IL20RA as a promising therapeutic target but also highlight the value of IL(R) genes to predicting prognosis for WT. To further substantiate these results, future research should prioritize validation in larger cohorts and investigate the role of *IL20RA* in targeted therapies, thereby refining treatment strategies for WT.

Materials and methods

Data acquisition

We downloaded the transcriptomic data and relevant clinical information from the TCGA database (https://portal.gdc.cancer.gov/) and normalized the raw count data with DESeq2 package to make the samples more comparable. The list of IL(R)s was obtained from the KEGG PATHWAY Database[45–47] (https://www.kegg.jp/kegg/pathway.html). The TARGET-WT cohort contained a total of 136 WT samples, consisting of 130 tumor tissue samples and 6 adjacent normal tissue samples. Inclusion criteria were as follows: Complete follow-up data available; Age below 16 years; Primary tumor samples at diagnosis, or matched normal tissue samples from peripheral blood and/or adjacent normal kidney tissue; Case-matched relapsed tumor sample; Tumor cell purity > 80% and tumor necrosis < 20% in tumor specimens; Sufficient quantity of high-quality nucleic acid for comprehensive genomic analysis. Following the exclusion of five recurrent tumor tissue samples, 125 tumor samples and 6 normal samples were included in the final analysis.

Screening of DEGs

The RNA expression data for both protein-coding and non-coding genes were used for downstream gene expression analysis. First and foremost, genes with a count per million equal to or less than 1 in at least 75% of the samples were excluded from further analysis. The "DESeq2" package (version 1.46.0) was employed for normalization and differential gene expression analyses between tumor tissues and normal tissues. Genes with $|\log FC| \geq 2$ and $p < 0.05$ were considered to have significant differences.

Construction and evaluation of the prognostic model

Prognosis-related IL(R)s were identified by univariate Cox regression analysis, setting $p < 0.05$ as statistically significant. Subsequently, LASSO regression ("glmnet" package, version 4.1-8) algorithms were used for model development. WT data were divided into "training" (80%) and "validation" (20%) sets. A model was built on the training set, and the dead risk was predicted using this model for subjects in the corresponding validation set. When $\log(\lambda) = -1.655$, 5 variables were selected to construct the final signature. The overall survival (OS) of the high-risk group and the low-risk group was compared using KM survival analysis and log-rank test. The area under the ROC curve (AUC) was calculated by the "pROC" package (version 1.18.4) to evaluate the predictive ability.

Moreover, IL(R)s-based signature and clinicopathological parameters (including age, gender, and stage) were analyzed by univariate and multivariate Cox regression analyses. Based on that, the prognostic signatures that can be considered independent risk factors were identified, and a prognostic model was constructed. The nomogram and calibration diagram were plotted to evaluate the prognosis (1-year, 3-year, and 5-year OS) of patients with WT.

Evaluation of immune characteristics

The stromal score and immune score of each sample were calculated by the ESTIMATE algorithm. The immune function of children in different risk groups was evaluated and compared by the "ssGSEA" algorithm, and the gene sets related to immune functions were downloaded from ImmPort Portal (https://www.immport.org/shared/genelists). TIDE scores and immunotherapy responsiveness were predicted using The Tumor Immune Dysfunction and Exclusion (TIDE) tool (http://tide.dfci.harvard.edu/).

Identification of IL(R)s-related clusters

IL(R)s related molecules subtypes were identified using ConsensusClusterPlus package with 1000 iterations, resample rate of 0.8. Kaplan–Meier (K-M) analysis was performed to compare the prognosis between the two clusters.

Cell culture

The HEK293T and WIT 49 cell lines (Shanghai Cell Bank, China) were separately maintained in Dulbecco's Modified Eagle Medium and McCoy's 5A modified medium, containing 10% fetal calf serum, 100 U/ml penicillin and 100 U/ml streptomycin, at 37 °C and 5% CO2. Both types of cells have been tested for mycoplasma and were Mycoplasma-Free.

Real-time fluorescence quantitative PCR

The total RNA was extracted from WIT 49 and HEK293 cells (220011, Fastagen, China). Then, the RNA was reverse transcription to obtain the complementary DNA (cDNA) by Evo M-MLV RT Kit with gDNA Clean for qPCR (AG11705, AG accurate biology, China). Subsequently, qRT-PCR was performed using SYBR Green Pro Taq HS Premix II (AG11702, AG accurate biology, China). The primer sequence is shown in supplementary materials (Table S6). The 2-ΔΔCT method was used to calculate the relative expression of genes.

Immunohistochemistry

Tumor tissues were embedded in paraffin wax, and serially sectioned to 3 μm. Sections were then examined for IL20RA expression with a polyclonal antibody (1:100) purchased from Proteintech, China. Polyclonal antibodies were detected by goat anti-rabbit IgG (Servicebio) and DAB chromogenic kit (Servicebio).

Plasmids construction

Two shRNAs targeting the IL19 gene were inserted into the PLKO.1 vector with the following sequences: 5′-CCGGCAGATCATTAAGCCCTTAGATCTCGAGATCTAAGGGCTTAATGATCTGTTTTTG-3′, 5′-AATTCAAAAACAGATCATTAAGCCCTTAGATCTCGAGATCTAAGGGCTTAATGATCTG-3′ (referred as 'sh-*IL19*-1'), 5′-CCGGGACGTCTTTCTAGCCTGGATTCTCGAGAATCCAGGCTAGAAAGACGTCTTTTTG-3′, 5′-AATTCAAAAAGACGTCTTTCTAGCCTGGATTCTCGAGAATCCAGGCTAGAAAGACGTC-3′ (referred as 'sh-*IL19*-2'). Two shRNAs targeting the IL20RA gene were inserted into the PLKO.1 vector with the following sequences: 5′-CCGGGCAAACATCACCTTCTTATCCCTCGAGGGATAAGAAGGTGATGTTTGCTTTTTG-3′, 5′-AATTCAAAAAGCAAACATCACCTTCTTATCCCTCGAGGGATAAGAAGGTGATGTTTGC-3′ (referred as 'sh-*IL20RA*-1'), 5′-CCGGGCCAGGACTTTGAAAGATCAACTCGAGTTGATCTTTCAAAGTCCTGGCTTTTTG-3′, 5′-AATTCAAAAAGCCAGGACTTTGAAAGATCAACTCGAGTTGATCTTTCAAAGTCCTGGC-3′ (referred as 'sh-*IL20RA*-2'). A PLKO.1 vector encoding scrambled shRNA sequence used as a negative control (referred as 'sh-NC'). The plasmid pCDNA 3.1(+) was used to construct control overexpression plasmid (referred as 'oe-NC'), *IL19* overexpression plasmid (referred as 'oe-*IL19*') and *IL20RA* overexpression plasmid (referred as 'oe-*IL20RA*'). The plasmids described above were transfected into Wit-49 cells by lipo2000 (Invitrogen), RNA and protein were extracted after 48 h, and functional experiments were performed.

CCK-8 assay
Twenty-four hours after the transfection, WIT 49 cells were planted in 96-well plates at a density of 2×10^3/100 µl per well. 10 µl of CCK-8 reagent (GLPBIO, USA) was added to each well at 0 h, 24 h, 48 h, and 72 h, respectively. Then, the absorbance of each well at 450 nm was determined two hours later.

Transwell assays
For the migration assay, 5×10^4 cells in 200 µl of McCoy's 5A modified medium were seeded into the upper transwell chamber. 600 µl of complete medium containing 20% FBS was added to the lower chamber. After 24-h incubation at 37 °C, the cells transferred into the lower chamber were fixed with methanol, and then stained with 1% crystal violet staining solution.

Scratch assay
The transfected cells were seeded in a 6-well plate, the incubation was continued at 37 °C till the cells reached 100% confluence. And then, cells were gently scrapped off along the ruler with a 200 µl pipette tip. The floating cells were washed thrice with PBS and placed in a medium containing 1% FBS. These cells in each group were then observed and photographed after 48 h. Percentage of wound healed was quantified by Image J.

Western blot
On the third day after transfection, total protein was extracted from cells using RIPA lysis buffer (Biyuntian, China), separated through a 4–12% polyacrylamide resolving gel (ACE, China), and transferred onto PVDF membranes (Biyuntian, China). Thereafter, blots were incubated with specific primary antibodies followed by an anti-rabbit secondary antibody. Finally, the membranes were visualized with ECL reagent and photographed (Beyotime, China). β-actin was used as the internal reference protein. The full-length blots were included in the Supplementary Info File "Full-length plots".

COIP
HEK293 cells were transfected with lipo2000 transfection reagent (Invitrogen) and the expression plasmid encoded the FLAG-IL20RA protein. The protein was extracted using Cell lysis buffer for Western and IP (Beyotime, China) and a mixture of protease inhibitors (Beyotime, China). Added 20ul of anti-FLAG magnetic beads or anti IgG magnetic beads suspension (Beyotime, China) to every 500ul protein sample and incubated overnight at 4 °C. Released bound proteins by adding protein loading buffer and boiling at 95 °C for 5 min. The fusion protein was detected by immunoblotting using anti-IL20RA (Abclonal Technology, China) and anti-STAT3 antibodies (Beyotime, China).

CHIP
The ChIP Assay Kit was used to conduct ChIP experiments (Beyotime, China). In short, the crude chromatin extract was divided into three parts. One part was saved as input control, while the other two parts were treated with anti-STAT3 (Beyotime, China) or anti IgG antibodies (Abclonal Technology, China). After several washes, purification was performed using a PCR purification kit (Beyotime, China). Perform real-time fluorescence quantitative PCR analysis using 1 µl of DNA. The sequences of ChIP-qPCR primer were shown in Table S7.

Subcutaneous tumor formation experiment in nude mice
The animal experiment was conducted following approval from the Animal Experiment Ethics Committee of Qilu Hospital of Shandong University (DWLL-2024-312). Ten five-week-old Nude mice (BALB/c nude), obtained from Beijing HFK bioscience CO., Ltd, were acclimated to a barrier environment for one week prior to the subcutaneous tumorigenesis experiments. After the injection of tumor cells, all eight nude mice developed tumors within one week. The tumor volumes were subsequently measured every three days, and these measurements were used to construct a tumor growth curve.

Statistical analysis
The vast majority of statistical analyses were performed in R v.4.1.2. Continuous variables were compared through the Wilcoxon test. The log-rank test was conducted to compare the Kaplan–Meier survival curves. Both Univariate- and multivariate Cox regression analyses were applied to identify factors associated with OS. All p values were two-side, and the significance level was 0.05. $^*p < 0.05$; $^{**}p < 0.01$; $^{***}p < 0.001$; $^{****}p < 0.0001$ and ns, not significant were displayed in the figures. Experiments were conducted with three replicates.

Data availability
The datasets generated during and/or analysed during the current study are available from the corresponding author on reasonable request.

Received: 26 November 2024; Accepted: 26 March 2025
Published online: 04 April 2025

References
1. Pater, L. et al. Wilms tumor. *Pediatr. Blood Cancer* **68 Suppl 2**, e28257. https://doi.org/10.1002/pbc.28257 (2021).
2. Kumar, A., Bakhshi, S. & Agarwala, S. Is pre-operative chemotherapy desirable in all patients of Wilms' tumor?. *Indian J Pediatr* **84**, 709–714. https://doi.org/10.1007/s12098-017-2410-5 (2017).
3. Hont, A. B. et al. The tumor microenvironment and immune targeting therapy in pediatric renal tumors. *Pediatr. Blood Cancer* **70 Suppl 2**, e30110. https://doi.org/10.1002/pbc.30110 (2023).

4. Jain, J., Sutton, K. S. & Hong, A. L. Progress update in pediatric renal tumors. *Curr. Oncol. Rep.* **23**, 33. https://doi.org/10.1007/s11912-021-01016-y (2021).
5. Wang, J., Li, D., Cang, H. & Guo, B. Crosstalk between cancer and immune cells: Role of tumor-associated macrophages in the tumor microenvironment. *Cancer Med.* **8**, 4709–4721. https://doi.org/10.1002/cam4.2327 (2019).
6. Zhang, C., Zhang, X. & Chen, X. H. Inhibition of the interleukin-6 signaling pathway: A strategy to induce immune tolerance. *Clin. Rev. Allergy Immunol.* **47**, 163–173. https://doi.org/10.1007/s12016-014-8413-3 (2014).
7. Huang, C. K. et al. Autocrine/paracrine mechanism of interleukin-17B receptor promotes breast tumorigenesis through NF-κB-mediated antiapoptotic pathway. *Oncogene* **33**, 2968–2977. https://doi.org/10.1038/onc.2013.268 (2014).
8. Hughes, T., Klairmont, M., Sharfman, W. H. & Kaufman, H. L. Interleukin-2, Ipilimumab, and Anti-PD-1: Clinical management and the evolving role of immunotherapy for the treatment of patients with metastatic melanoma. *Cancer Biol. Ther.* **22**, 513–526. https://doi.org/10.1080/15384047.2015.1095401 (2021).
9. Lopatina, T. et al. Targeting IL-3Rα on tumor-derived endothelial cells blunts metastatic spread of triple-negative breast cancer via extracellular vesicle reprogramming. *Oncogenesis* **9**, 90. https://doi.org/10.1038/s41389-020-00274-y (2020).
10. Liguori, M. et al. The soluble glycoprotein NMB (GPNMB) produced by macrophages induces cancer stemness and metastasis via CD44 and IL-33. *Cell Mol. Immunol.* **18**, 711–722. https://doi.org/10.1038/s41423-020-0501-0 (2021).
11. Xu, Y. et al. Regulatory T cells promote the stemness of leukemia stem cells through IL10 cytokine-related signaling pathway. *Leukemia* **36**, 403–415. https://doi.org/10.1038/s41375-021-01375-2 (2022).
12. Yang, L. et al. IL-10 derived from M2 macrophage promotes cancer stemness via JAK1/STAT1/NF-κB/Notch1 pathway in non-small cell lung cancer. *Int. J. Cancer* **145**, 1099–1110. https://doi.org/10.1002/ijc.32151 (2019).
13. Kobayashi, T. et al. Regulatory B1a cells suppress melanoma tumor immunity via IL-10 production and inhibiting T helper type 1 cytokine production in tumor-infiltrating CD8(+) T cells. *J. Invest. Dermatol.* **139**, 1535-1544.e1531. https://doi.org/10.1016/j.jid.2019.02.016 (2019).
14. Sciesielski, L. K., Kirschner, K. M., Scholz, H. & Persson, A. B. Wilms' tumor protein Wt1 regulates the Interleukin-10 (IL-10) gene. *FEBS Lett.* **584**, 4665–4671. https://doi.org/10.1016/j.febslet.2010.10.045 (2010).
15. Cheng, B. et al. Single-cell deconvolution algorithms analysis unveils autocrine IL11-mediated resistance to docetaxel in prostate cancer via activation of the JAK1/STAT4 pathway. *J. Exp. Clin. Cancer Res.* **43**, 67. https://doi.org/10.1186/s13046-024-02962-8 (2024).
16. Mathios, D. et al. Therapeutic administration of IL-15 superagonist complex ALT-803 leads to long-term survival and durable antitumor immune response in a murine glioblastoma model. *Int. J. Cancer* **138**, 187–194. https://doi.org/10.1002/ijc.29686 (2016).
17. Teng, M. W., Darcy, P. K. & Smyth, M. J. Stable IL-10: A new therapeutic that promotes tumor immunity. *Cancer Cell* **20**, 691–693. https://doi.org/10.1016/j.ccr.2011.11.020 (2011).
18. Fan, T. et al. Clinical significance and immunologic landscape of a five-IL(R)-based signature in lung adenocarcinoma. *Front Immunol.* **12**, 693062. https://doi.org/10.3389/fimmu.2021.693062 (2021).
19. Ni, S., Shan, F. & Geng, J. Interleukin-10 family members: Biology and role in the bone and joint diseases. *Int. Immunopharmacol.* **108**, 108881. https://doi.org/10.1016/j.intimp.2022.108881 (2022).
20. Hsing, C. H. et al. Upregulated IL-19 in breast cancer promotes tumor progression and affects clinical outcome. *Clin. Cancer Res.* **18**, 713–725. https://doi.org/10.1158/1078-0432.Ccr-11-1532 (2012).
21. Richards, J. et al. Interleukin-19 increases angiogenesis in ischemic hind limbs by direct effects on both endothelial cells and macrophage polarization. *J. Mol. Cell Cardiol.* **79**, 21–31. https://doi.org/10.1016/j.yjmcc.2014.11.002 (2015).
22. Khare, V. et al. IL10R2 overexpression promotes IL22/STAT3 signaling in colorectal carcinogenesis. *Cancer Immunol. Res.* **3**, 1227–1235. https://doi.org/10.1158/2326-6066.Cir-15-0031 (2015).
23. Dumoutier, L., Leemans, C., Lejeune, D., Kotenko, S. V. & Renauld, J. C. Cutting edge: STAT activation by IL-19, IL-20 and mda-7 through IL-20 receptor complexes of two types. *J. Immunol.* **167**, 3545–3549. https://doi.org/10.4049/jimmunol.167.7.3545 (2001).
24. Gabunia, K. et al. IL-19 halts progression of atherosclerotic plaque, polarizes, and increases cholesterol uptake and efflux in macrophages. *Am. J. Pathol.* **186**, 1361–1374. https://doi.org/10.1016/j.ajpath.2015.12.023 (2016).
25. Kako, F. et al. Interleukin-19 induces angiogenesis in the absence of hypoxia by direct and indirect immune mechanisms. *Am. J. Physiol. Cell Physiol.* **310**, C931-941. https://doi.org/10.1152/ajpcell.00006.2016 (2016).
26. Lai, X. et al. IL-19 up-regulates mucin 5AC production in patients with chronic rhinosinusitis via STAT3 pathway. *Front Immunol.* **10**, 1682. https://doi.org/10.3389/fimmu.2019.01682 (2019).
27. He, Y. et al. IL-20RB mediates tumoral response to osteoclastic niches and promotes bone metastasis of lung cancer. *J. Clin. Invest.* **132**, e157917. https://doi.org/10.1172/jci157917 (2022).
28. Yu, D. et al. Super-enhancer induced IL-20RA promotes proliferation/metastasis and immune evasion in colorectal cancer. *Front Oncol.* **11**, 724655. https://doi.org/10.3389/fonc.2021.724655 (2021).
29. Maciaszek, J. L., Oak, N. & Nichols, K. E. Recent advances in Wilms' tumor predisposition. *Hum. Mol. Genet.* **29**, R138-r149. https://doi.org/10.1093/hmg/ddaa091 (2020).
30. Watson, T., Oostveen, M., Rogers, H., Pritchard-Jones, K. & Olsen, Ø. The role of imaging in the initial investigation of paediatric renal tumours. *Lancet Child Adolesc. Health* **4**, 232–241. https://doi.org/10.1016/s2352-4642(19)30340-2 (2020).
31. Dome, J. S. et al. Impact of the first generation of children's oncology group clinical trials on clinical practice for Wilms tumor. *J. Natl. Compr. Cancer Netw.* **19**, 978–985. https://doi.org/10.6004/jnccn.2021.7070 (2021).
32. Akimoto, M. & Takenaga, K. Role of the IL-33/ST2L axis in colorectal cancer progression. *Cell Immunol.* **343**, 103740. https://doi.org/10.1016/j.cellimm.2017.12.014 (2019).
33. Lee, J. E. et al. The role of interleukin-9 in cancer. *Pathol. Oncol. Res.* **26**, 2017–2022. https://doi.org/10.1007/s12253-019-00665-6 (2020).
34. Mizui, M. Natural and modified IL-2 for the treatment of cancer and autoimmune diseases. *Clin. Immunol.* **206**, 63–70. https://doi.org/10.1016/j.clim.2018.11.002 (2019).
35. Cao, X. et al. Stat3 inhibits WTX expression through up-regulation of microRNA-370 in Wilms tumor. *FEBS Lett.* **587**, 639–644. https://doi.org/10.1016/j.febslet.2013.01.012 (2013).
36. Tian, X. M. et al. Immune-related gene signature associates with immune landscape and predicts prognosis accurately in patients with Wilms tumour. *Front. Immunol.* **13**, 920666. https://doi.org/10.3389/fimmu.2022.920666 (2022).
37. Higgs, E. F., Bao, R., Hatogai, K. & Gajewski, T. F. Wilms tumor reveals DNA repair gene hyperexpression is linked to lack of tumor immune infiltration. *J. Immunother. Cancer* https://doi.org/10.1136/jitc-2022-004797 (2022).
38. Li, J. et al. A systematic CRISPR screen reveals an IL-20/IL20RA-mediated immune crosstalk to prevent the ovarian cancer metastasis. *Elife* https://doi.org/10.7554/eLife.66222 (2021).
39. Lamichhane, S., Mo, J. S., Sharma, G., Choi, T. Y. & Chae, S. C. MicroRNA 452 regulates IL20RA-mediated JAK1/STAT3 pathway in inflammatory colitis and colorectal cancer. *Inflamm. Res.* **70**, 903–914. https://doi.org/10.1007/s00011-021-01486-7 (2021).
40. Deng, Y. et al. Preclinical analysis of novel prognostic transcription factors and immune-related gene signatures for bladder cancer via TCGA-based bioinformatic analysis. *Oncol. Lett.* **21**, 344. https://doi.org/10.3892/ol.2021.12605 (2021).
41. Swarts, D. R. et al. An exploration of pathways involved in lung carcinoid progression using gene expression profiling. *Carcinogenesis* **34**, 2726–2737. https://doi.org/10.1093/carcin/bgt271 (2013).
42. Gao, W. et al. IL20RA signaling enhances stemness and promotes the formation of an immunosuppressive microenvironment in breast cancer. *Theranostics* **11**, 2564–2580. https://doi.org/10.7150/thno.45280 (2021).

43. Chiriac, M. T. et al. IL-20 controls resolution of experimental colitis by regulating epithelial IFN/STAT2 signalling. *Gut* **73**, 282–297. https://doi.org/10.1136/gutjnl-2023-329628 (2024).
44. Keller, K. E., Yang, Y. F., Sun, Y. Y., Walter, M. R. & Wirtz, M. K. Analysis of interleukin-20 receptor complexes in trabecular meshwork cells and effects of cytokine signaling in anterior segment perfusion culture. *Mol. Vis.* **25**, 266–282 (2019).
45. Kanehisa, M., Furumichi, M., Sato, Y., Kawashima, M. & Ishiguro-Watanabe, M. KEGG for taxonomy-based analysis of pathways and genomes. *Nucleic Acids Res.* **51**, D587-d592. https://doi.org/10.1093/nar/gkac963 (2023).
46. Kanehisa, M. & Goto, S. KEGG: Kyoto encyclopedia of genes and genomes. *Nucleic Acids Res.* **28**, 27–30. https://doi.org/10.1093/nar/28.1.27 (2000).
47. Kanehisa, M. Toward understanding the origin and evolution of cellular organisms. *Protein Sci.* **28**, 1947–1951. https://doi.org/10.1002/pro.3715 (2019).

Acknowledgements
We would like to acknowledge support and resources provided by the Stomatology Laboratory, Shandong University.

Author contributions
Chen Ding: Conceptualization (Equal), Data curation (Equal), Project administration (Equal), Writing—original draft (Equal), Writing—review & editing (Equal); Hongjie Gao: Data curation (Equal), Formal analysis (Equal), Methodology (Equal), Validation (Equal); Liting Zhang: Investigation (Equal), Software (Equal), Visualization (Equal); Zhiyi Lu: Investigation (Equal), Methodology (Equal), Validation (Equal); Bowen Zhang: Formal analysis (Equal), Investigation (Equal), Methodology (Equal); Ding Li: Resources (Equal), Software (Equal), Validation (Equal); Fengyin Sun: Conceptualization (Equal), Funding acquisition (Equal), Methodology (Equal), Resources (Equal), Supervision (Equal), Writing—review & editing (Equal).

Funding
This work was supported by Grant ZR2020MH076 from Natural Science Foundation of Shandong Province, and by Grant 6010121111 from Horizontal project of Shandong Qidu Pharmaceutical Co., Ltd.

Declarations

Competing interests
The authors declare no competing interests.

Ethics approval
This study was performed in line with the principles of the Declaration of Helsinki. Approval was granted by the Ethics Committee of Qilu Hospital of Shandong University (July 7, 2023/KYLL-202212-031). Informed consent was obtained from the subjects and or their parents/legal guardians.

ARRIVE guidelines statement
Our study was reported in accordance with the ARRIVE (Animal Research: Report-ing In Vivo Experiments) guidelines and in accordance with relevant guidelines and regulations.

Additional information
Supplementary Information The online version contains supplementary material available at https://doi.org/10.1038/s41598-025-96094-4.

Correspondence and requests for materials should be addressed to F.S.